Lodi Agriculture

Leveraging NASA Earth Observations to Detect Vine Stress and Potential Viral Presence in Vineyards to Inform Management Decisions

Fall 2025 | California – Ames
November 21st 2025

Authors: Audrey Chin (Analytical Mechanics Associates), Noah Larkin (Analytical Mechanics Associates), Derek Gonzalez (Analytical Mechanics Associates), Monica Napoles Serrano (Analytical Mechanics Associates)

Abstract:
Grapevine leafroll-associated virus complex 3 (GLRaV-3) is one of the most damaging viral grapevine diseases in the world. This virus represents a pressing concern for the Lodi Winegrape Commission (LWC), a viticultural organization based in northern California. Traditional GLRaV-3 detection methods are generally time-intensive and expensive, further complicating mitigation efforts. We partnered with the LWC, NASA Acres, and the Gold Lab at Cornell University to create and test a scalable GLRaV-3 detection model using Earth observations. We explored hyperspectral imagery from the Earth Surface Mineral Dust Source Investigation (EMIT) and multispectral imagery from the Sentinel-2 Multispectral Instrument from August and September 2022–2024. For EMIT, we ran a Principal Component Analysis (PCA) to reduce dimensionality and identify components representing maximum variance. For Sentinel-2, we calculated indices including the Normalized Difference Red Edge Index (NDRE) and Plant Senescence Reflectance Index (PSRI) to extract additional information about vegetation health. Using random forest classification models and ground-truth scouting data, we classified vineyard areas based on GLRaV-3 symptom presence. Due to training data limitations and differences in spatial resolution between sensors, we employed a binary symptomatic/unknown status classification for Sentinel-2 and a threshold-based classification (above or below 1% symptomatic rate) for EMIT. Results demonstrated that the EMIT model was more sensitive to areas of higher symptomatic vine density than the Sentinel-2 model, suggesting that hyperspectral data may be more suitable than multispectral for GLRaV-3 associated symptom mapping. This indicates that spectral resolution may be more critical than spatial resolution for this application.

Key Terms: remote sensing, Sentinel-2, EMIT, grapevine leafroll-associated virus complex 3 (GLRaV-3), hyperspectral, viticulture, agriculture

Advisors: Dr. Morgan Gilmour (NASA Ames Research Center), Dr. Dana Chadwick (NASA Jet Propulsion Lab)

Lead: Katie Miller (California – Ames)

1. Introduction

Grapevine leafroll-associated virus complex 3 (GLRaV-3) causes economic losses for winegrape growers due to decreases in grape yield and reduced fruit quality (Bolton, 2020). California's 2023 grape production valuation was $6.5 billion, making potential for loss a significant economic concern for growers (California Department of Food and Agriculture, 2024). The primary vector of GLRaV-3 is the invasive vine mealybug, *Planococcus ficus,* which reproduces rapidly, spreads via wind, hides under bark and on roots, and even has a symbiotic relationship with ants. One single mealybug can infect a vine with GLRaV-3 in under an hour (Australian Wine Research Institute, 2021; Bolton, 2020). In red grape cultivars, GLRaV-3 infection manifests through physiological changes like leaf reddening and rolling of leaf margins, enabling visual identification of the disease. However, due to disease latency, vines can be infected and not show visible symptoms. White grape cultivars generally show subtle to no symptoms but can exhibit leaf curling in severe cases (Maree et al., 2013). GLRaV-3 is difficult to manage due to the quick-growing mealybug population, which compounds yearly. This is exacerbated by the cost and regulation of chemical treatments and the disease latency period, which delays the identification of virus presence. This is a billion-dollar problem for winegrowers, as identification of viral disease through molecular testing or scouting methods is costly and difficult to scale (Bolton, 2023). Earth observations (EO) could enable scalable detection by identifying physiological and chemical changes to grapevine systems, informing disease management decisions, easing costs, and lowering the risk of plant loss (Romero Galvan et al., 2023). Lodi, California has been the site of previous research leveraging EOs to attempt to detect GLRaV-3 (Figure 1).

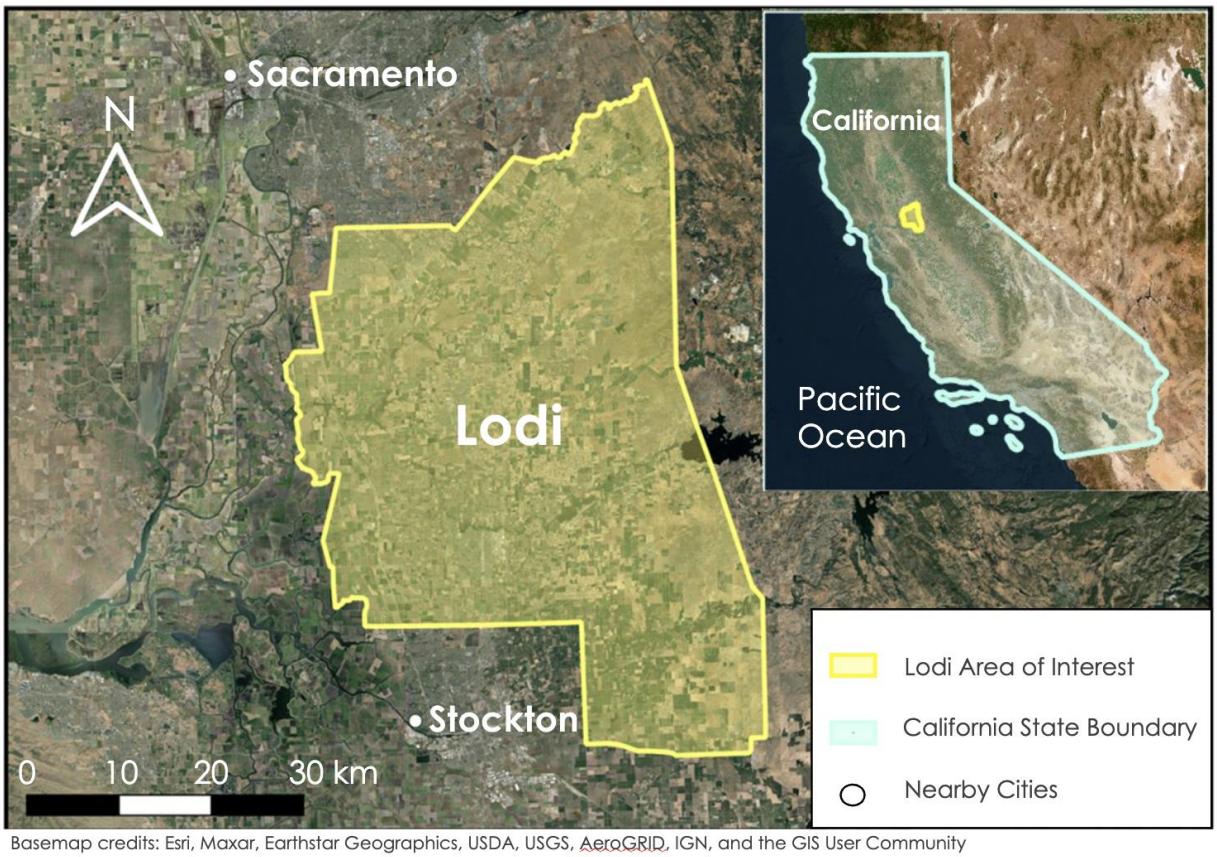

Figure 1: True color image with Lodi study area and geographic reference map of California.

Lodi is one of California's leading wine-producing areas, known for having over 130 different grape varieties, including its famous Zinfandel old vines. The Mediterranean climate of this region brings warm, dry summers and cool, wet winters, which benefit quality grape production. Widespread, close plantings make vineyards

more susceptible to pests and viral diseases, including GLRaV-3 (Lodi Winegrape Commission, 2025). A prior study using data collected in Lodi by the NASA Airborne Visible/Infrared Imaging Spectrometer Next Generation (AVIRIS-NG) revealed spectral differences for differentiating between non-infected, symptomatic, and asymptomatic vines. This was achieved using a random forest model validated by on-the-ground scouting and molecular testing in September 2020 and 2021 (Romero Galvan et al., 2023).

Hyperspectral imaging is a useful remote sensing tool for plant disease identification as it can detect fine-scale spectral differences in stressed plants. Previous grapevine viral disease identification studies have combined hyperspectral data with in situ measurements to train machine learning models like convolutional neural networks and random forest models (Nguyen et al., 2021; Sawyer et al., 2023). Generally, random forest models are well-performing and widely used for plant-microbe interaction sensing (Portela et al., 2024). Nevertheless, airborne hyperspectral flights are expensive and have a lower temporal frequency than satellite-based sensors; therefore, investigating the use of cheaper and more frequent hyperspectral and multispectral imagery can help fill gaps. The primary project objective was to evaluate the feasibility of using NASA's Earth Surface Mineral Dust Source Investigation (EMIT) and the European Space Agency's (ESA) Sentinel-2 Multispectral Instrument (MSI), satellite-based sensors with coarser spatial but finer temporal resolution, to identify GLRaV-3 and map viral presence and spread across Lodi from 2022–2024.

We examined vineyards located throughout the Lodi wine region with satellite imagery and scouting data from August and September, 2022–2024. The selected timeframe was ideal for GLRaV-3 symptom detection as symptoms peak in the fall. Specifically, red grape varieties display crucial viral stress indicators through leaf reddening and rolling (Caparoso, 2024).

We partnered with the Lodi Winegrape Commission (LWC), an organization dedicated to supporting the approximately 750 winegrowers of the greater Lodi region through education, marketing, research, and sustainable viticulture initiatives (Bolton, 2020; LWC, 2025). The LWC has previously employed multiple strategies to improve GLRaV-3 detection and awareness, including running a canine detection pilot study, writing a grower-oriented book on mealybugs and grapevine viruses, and facilitating field scouting and lab testing efforts (Bolton, 2023; Bolton, 2025). The results of this study provided the LWC with updated information on GLRaV-3 detection, supporting their efforts to educate growers about viral diseases, and deepening their understanding of the feasibility of GLRaV-3 monitoring using hyperspectral and multispectral satellites. We also worked in collaboration with NASA Acres, a consortium that leverages satellite data to strengthen the U.S. agrifood system, as well as with the Gold Lab at Cornell University, which conducts plant pathology research to support vineyard disease management.

2. Methods

2.1 Data Acquisition

To create a scalable model that predicted GLRaV-3 incidence from 2022–2024 in Lodi, CA, we assessed the suitability of two EO datasets provided by NASA and ESA respectively. We utilized two primary data sources, filtering imagery to the study periods of August and September: (1) the EMIT L2A Surface Reflectance and Uncertainty and Masks dataset, accessed through the NASA earthaccess API; and (2) the Harmonized Sentinel-2 MSI Level-2A Surface Reflectance dataset, accessed through Google Earth Engine (GEE; Table 1).

Local stakeholders shared ground-truth vine scouting data with the Gold Lab to conduct their NASA-funded and affiliated research projects. The Gold Lab supplied us with these data for the purposes of this DEVELOP project. Trained field technicians scouted grapevines annually from 2017–2025. Scouts were trained to recognize symptoms of GLRaV-3, geotag symptomatic vines, and collect samples to send to the testing facility for verification on a subset of scouted plants. Scouting was performed exclusively in vineyards with red grape varieties, with scouted vineyards covering approximately 5.1 square kilometers with small variation year to year.

Table 1. Data source information

Source	Data Product	Dates	Acquisition Method	DOI
ISS EMIT	EMIT L2A Estimated Surface Reflectance and Uncertainty and Masks (60 m)	8/1–9/30, 2022–2024	NASA earthaccess API	Green, R. (2022). *EMIT L2A Estimated Surface Reflectance and Uncertainty and Masks 60 m V001* [Data set]. NASA Land Processes Distributed Active Archive Center. https://doi.org/10.5067/EMIT/EMITL2ARFL.001 Date Accessed: 2025-09-22
Sentinel-2 MSI	Harmonized Sentinel-2 MSI: MultiSpectral Instrument, Level-2A (SR) (10 m)	8/1–9/30, 2022–2024	Google Earth Engine Data Catalog	Copernicus Sentinel data (2024). *Harmonized Sentinel-2 MSI: MultiSpectral Instrument, Level-2A (SR) (10 m)*. Copernicus Data Space Ecosystem – STAC API. http://doi.org/10.5270/S2_-znk9xsj Date Accessed: 2025-09-22
Alcohol and Tobacco Tax and Trade Bureau	Lodi AVA Shapefile	2025	AVA Map Explorer	Alcohol and Tobacco Tax and Trade Bureau (2025). *Lodi AVA Shapefile* [Dataset]. U.S. Department of Treasury. https://www.ttb.gov/regulated-commodities/beverage-alcohol/wine/ava-map-explorer Date Accessed: 2025-09-22
California Department of Water Resources	Provisional 2023 Statewide Crop Mapping GIS Shapefile	2023	California Natural Resources Agency Open Data	California Department of Water Resources. (2023). *Provisional 2023 Statewide Crop Mapping GIS Shapefile* [Dataset]. California Natural Resources Agency Open Data. https://data.cnra.ca.gov/dataset/statewide-crop-mapping Date Accessed: 2025-09-29

2.2 Data Processing

We applied various processing and analysis workflows for the EMIT and Sentinel-2 datasets, using a combination of Python (Version 3.12.2), QGIS (Version 3.42), and the GEE Code Editor. Processing methodologies differed between EMIT and Sentinel-2 to account for differences in spatial and spectral resolution. In QGIS, we rasterized the 2022–2024 vineyard scouting data to match the 60 m spatial resolution of EMIT and the 2024 vineyard scouting data to match the 10 m spatial resolution of Sentinel-2. Each pixel in a scouted vineyard was assigned a value equal to the number of symptomatic vines it contained, and each pixel outside of a scouted vineyard was assigned a NaN value. We reprojected the scouting data rasters as needed to ensure pixel alignment with EMIT and Sentinel-2 imagery.

2.2.1 EMIT Data Processing

The EMIT L2A Surface Reflectance product comes in a non-georectified format. We explored the file format using the h5netcdf library (h5netcdf developers, 2025). The main dataset in the .nc file contains reflectance data organized by crosstrack, downtrack, and band dimensions. The .nc file also contains a geographic lookup table (GLT). We used the GLT to reproject the raw data into a georectified grid with a custom EMIT

processing library made by NASA called emit_tools (Bolch, 2024). Then, we applied cloud, cirrus, and water masks. Using EMIT masking bands, we removed any pixel flagged as containing cloud, cirrus, or water.

We then excluded bands with strong atmospheric absorption features where the surface reflectance cannot be accurately estimated. Following the methodology of Romero Galvan et al. (2023), we removed wavelengths from ~380 nm to ~400 nm, ~1310 nm to ~1470 nm, ~1750 nm to ~2000 nm, and ~2400 nm to ~2600 nm. Since EMIT bands are 7.4 nm wide and do not align precisely with these ranges, we removed any band with spectral overlap within the specified intervals. Reflectance values that contained a value of -9999 were replaced with a NaN.

Once the imagery was cleaned, we used rasterio to create geospatial transforms and write the dataset in a GeoTIFF format (Gillies et al., 2013). Next, we mosaiced multiple overlapping granules, using a median reducer. To improve accuracy, we reprojected from the coordinate reference system WGS84 (EPSG:4326) to UTM Zone 10N (EPSG:32610), using the bilinear resampling method. UTM Zone 10N covers a 6-degree band of longitude, from 126° W to 120° W, which includes a large portion of western California. The UTM projection minimizes distortion in the east-west direction, particularly accurately in narrow regions like Lodi, CA (Yildirim et. al., 2008). Finally, we clipped the imagery to the vineyard study area boundary, which was derived from the California Department of Water Resources provisional 2023 statewide crop map (Table 1; California Department of Water Resources, 2023).

2.2.2 Sentinel-2 Data Processing

GEE Sentinel-2 L2A data are orthorectified with top of atmosphere reflectance scaled by 1000. To filter the image to our area of interest, we filtered images that did not intersect with our shapefile for scouted vineyards in 2024. After scaling reflectance by dividing values by 1000, we set cloud probability to 25% to minimize cloud cover. We applied further masking using the scene classification layer. A binary value of zero was indicated for: cloud shadows, medium and high cloud probability, cirrus clouds, snow/ice, and water. We reduced our image collection by taking the median of our inputs, and the final composite image was reprojected to a CRS of WGS UTM Zone 10N with a scale of 10 m.

2.3 Data Analysis

2.3.1 Feature Calculations and Data Resampling

Due to the differing spectral resolutions of EMIT and Sentinel-2, we applied different techniques to calculate features for the random forest models. Because EMIT is high-dimensionality hyperspectral data, we applied a principal component analysis (PCA) to reduce the dimensionality of the feature space. As Sentinel-2 is multispectral and has fewer bands, we used index calculations to expand the number of features.

Prior to running the PCA, we took the processed 2022, 2023, and 2024 EMIT imagery and applied Normalized Difference Vegetation Index (NDVI) masks for each year, setting all pixels with an NDVI value less than 0.3 to a NaN value. The purpose of the NDVI mask was to remove pixels in vineyards that were not actively cultivated or mostly soil, as we wanted the PCA to identify variation across pixels with grapevine canopy. We then performed a PCA in Python on the 2022–2024 NDVI-masked EMIT imagery using the scikit-learn library (Pedregosa et al., 2011). We selected the first ten principal components to use as features for the EMIT-based random forest model. We chose ten because it is a standard number of principal components and explained most of the variation in the dataset.

To create additional features for the Sentinel-2 based random forest model, we calculated and tested five vegetation indices. These included NDVI (Equation 1; Kriegler et al., 1969), Plant Senescence Reflectance Index (PSRI; Equation 2; Merzlyak et al., 1999), Enhanced Vegetation Index (EVI; Equation 3; Huete et al., 2002), Normalize Difference Red Edge (NDRE; Equation 4; Barnes et al., 2000), and Normalized Difference Water Index (NDWI; Equation 5; McFeeters, 1996). We selected these indices based on their utility for detecting vegetation and plant stress to supplement the Sentinel-2 spectral bands.

$$NDVI = \frac{(NIR - Red)}{(NIR + Red)} \quad (1)$$

$$PSRI = \frac{(Red - Green)}{NIR} \quad (2)$$

$$EVI = Green \cdot \left(\frac{(NIR - Red)}{(NIR + C1 \cdot Red - C2 \cdot Blue + L)}\right) \quad (3)$$

$$NDRE = \frac{(NIR - RedEdge)}{(NIR + RedEdge)} \quad (4)$$

$$NDWI = \frac{(Green - NIR)}{(Green + NIR)} \quad (5)$$

For both EMIT and Sentinel-2, we matched the selected features with the rasterized scouting data, removing any pixels that did not have a valid scouting data value. For EMIT, this resulted in a dataset that included ten principal components and the scouting data. For Sentinel-2, this resulted in a dataset that included ten Sentinel-2 spectral bands, NDVI, PSRI, EVI, NDRE, NDWI, and the scouting data. Due to scouting data limitations, we grouped the scouting data values into binary classes. For Sentinel-2, we assigned pixels with no symptomatic vines to class 0 and assigned pixels with ≥1 symptomatic vines to class 1. This resulted in a total of 47,880 class 0 pixels and 3,231 class 1 pixels for Sentinel-2. For EMIT, we assigned pixels with <23 symptomatic vines to class 0 and ≥24 symptomatic vines to class 1. We chose 24 vines as a cutoff based on an assumption of 1-meter between vine spacing and 1.5-meter between row spacing (approximating 2,400 vines per 60 by 60 meter EMIT pixel), with class 0 approximately representing pixels with <1% symptomatic vines and class 1 approximately representing pixels with ≥1% symptomatic vines. This resulted in a total of 3,440 class 0 pixels and 135 class 1 pixels for EMIT.

For EMIT, we set aside 20 percent of the overall dataset for validation of our final model and used the remaining 80 percent for training and testing. The 80 percent was used to create ten random stratified 70-30 train-test splits. Because the data were extremely skewed toward class 0, we used heavy undersampling of the majority class (class 0) to achieve more balanced classes. For each train-test split, we performed cluster centroids undersampling with a 0.5 sampling strategy on the training set to achieve a more balanced data distribution using the Imbalanced-learn library (Lemaitre et al., 2017). This resampled each training set from 1,926 class 0 pixels and 76 class 1 pixels to a more balanced training set of 152 class 0 pixels and 76 class 1 pixels. We selected cluster centroids undersampling to address the class imbalance because it preserves the structure of the majority class while undersampling. We did not oversample our minority class to avoid potential for overfitting.

For Sentinel-2, 70 percent of our dataset was used for training, and the remaining 30 percent was used for testing our final model. However, our dataset exhibited severe class imbalance, with non-symptomatic pixels (class 0) heavily outweighing the number of symptomatic pixels (class 1). To address this issue, we performed random undersampling with a 0.20 sampling strategy on the training set to preserve all symptomatic samples while reducing the non-symptomatic samples using the Imbalanced-learn library (Lemaitre et al., 2017). We chose random undersampling rather than oversampling to avoid potential overfitting of the minority class, as

artificially generating symptomatic samples could introduce patterns not representative of true GLRaV-3 spectral signatures. This approach maintained 986 symptomatic pixels and undersampled the non-symptomatic class to 4,930 pixels in the training set, creating a more balanced distribution.

2.3.2 Random Forest Modeling

After preparing the feature data for EMIT and Sentinel-2, we initialized random forest classifier models with 100 trees. For Sentinel-2, our full model incorporated all 10 bands plus PSRI and NDRE. We decided on those two indices after running a feature importance analysis which showed that PSRI and NDRE had the most importance out of all indices. For EMIT, the ten principal components from the PCA served as the features for the random forest model. Each of the ten 70-30 train-test splits was used to train (using the undersampled training set) and evaluate (using the corresponding testing set) a random forest model, creating a model set. We chose the best performing model out of the model set, selected to maximize class 1 recall and precision, as the final EMIT random forest model. To assess model performance, we applied the trained Sentinel-2 model to the testing dataset and the final EMIT model to the validation dataset and calculated accuracy, recall, precision, and F1-score. We then applied the trained models to imagery for each sensor from 2022–2024 to model symptomatic vine presence over time across the full study area.

3. Results

3.1 Analysis of Results

3.1.1 Analysis of EMIT Results

The PCA of NDVI-masked EMIT imagery of Lodi vineyards from 2022–2024 yielded ten principal components that cumulatively explained ~99.94% of the variance in the dataset. The cumulative explained variance of each principal component is reported in Table 2. The principal components from the PCA became the features for the random forest classifier.

Table 2: Cumulative explained variance of principal components from PCA of EMIT imagery

Principal Component (PC)	**PC1**	**PC2**	**PC3**	**PC4**	**PC5**	**PC6**	**PC7**	**PC8**	**PC9**	**PC10**
Cumulative Explained Variance* (%)	68.22	90.17	98.17	99.24	99.72	99.80	99.86	99.90	99.92	99.94

*Values are rounded to four significant figures

The best performing random forest model from the model set yielded the following performance metrics when evaluated on the validation dataset. Overall accuracy was ~90.5%, precision for class 0 was ~98.9%, precision for class 1 was ~24.7%, recall for class 0 was ~91.1%, and recall for class 1 was ~74.1%. These metrics were calculated from the confusion matrix shown in Figure 2. For class 1, recall was much better than precision, indicating that pixels that had ≥1% symptomatic vines were likely to be correctly classified as such, but out of all the pixels classified as ≥1% symptomatic vines, the majority were false positives. The F1 score, calculated as the harmonic mean of precision and recall, was 0.37, reflecting the imbalance between the model's high class 1 recall and low class 1 precision. Relative feature importances for the model are reported in Table 3.

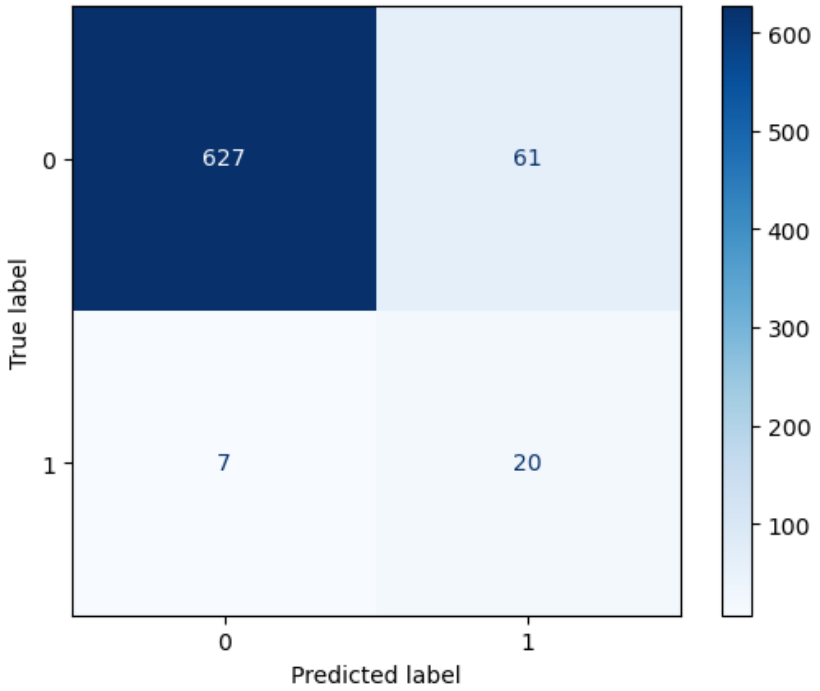

Figure 2: Confusion matrix of best performing EMIT-trained random forest model evaluated on validation dataset. Class 0 includes pixels with <1% symptomatic vines and class 1 includes pixels with ≥1% symptomatic vines.

Table 3: EMIT Random Forest Model Feature Importance

Principal Component (PC)	**PC1**	**PC2**	**PC3**	**PC4**	**PC5**	**PC6**	**PC7**	**PC8**	**PC9**	**PC10**
Feature Importance (%)	11.27	6.400	7.233	11.39	9.276	16.42	7.187	6.888	17.31	6.628

*Values are rounded to four significant figures

The best performing random forest model, applied to PCA-transformed imagery of Lodi vineyards from 2022–2024 yielded the maps displayed in Figure 3. To explore whether there were spatial trends in where the model misclassified pixels, we also visualized model accuracy for a subset of Lodi with scouting data (Figures A1–A3). We did not see obvious spatial patterns related to where the model misclassified pixels.

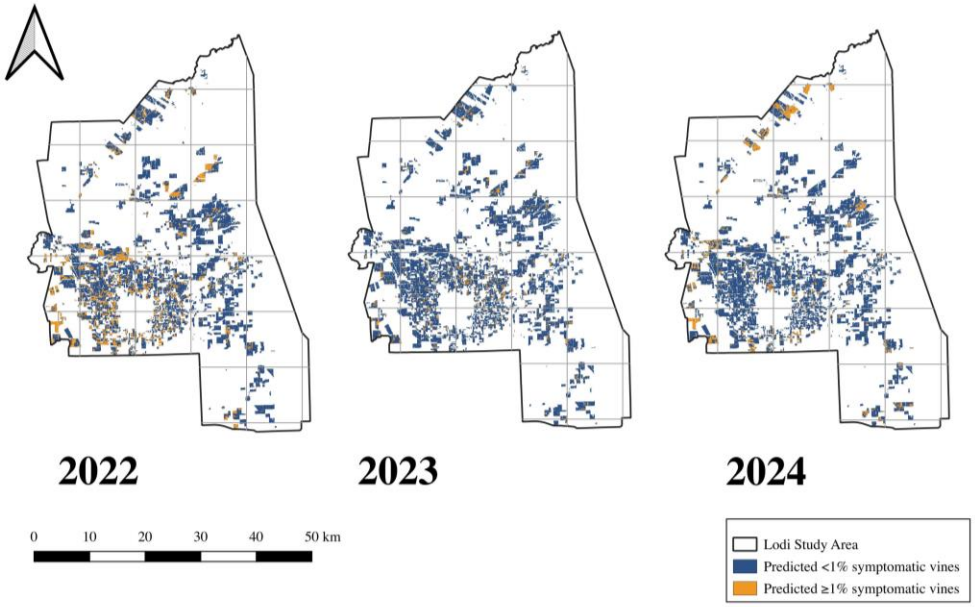

Figure 3: EMIT random forest model predictions for GLRaV-3 symptomatic classes. Model predictions were made by applying the best performing random forest model to PCA-transformed EMIT imagery of Lodi vineyards from August and September, 2022–2024.

3.1.2 *Analysis of Sentinel-2 Results*

Our binary classification model achieved 92.4% overall accuracy on the test set. However, this high accuracy masked significant limitations in detecting infected vines. The confusion matrix (Figure 4) revealed that out of the 15,334 pixels in our test set, our model correctly identified 13,846 non-symptomatic pixels (true negatives) and 322 symptomatic pixels (true positives) but misclassified 664 symptomatic pixels as non-symptomatic (false negatives) and 517 non-symptomatic pixels as symptomatic (false positives). Figure 5 displays a side by side comparison of scouting data and Sentinel-2 model predictions for 2024, illustrating model performance.

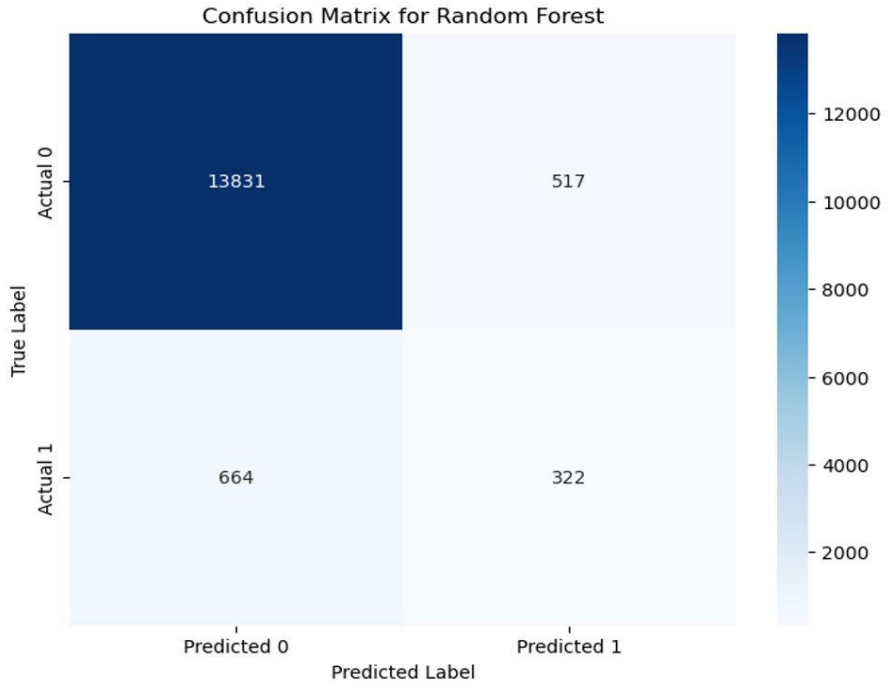

Figure 4: Confusion matrix of best performing Sentinel-2 trained random forest model evaluated on validation dataset.

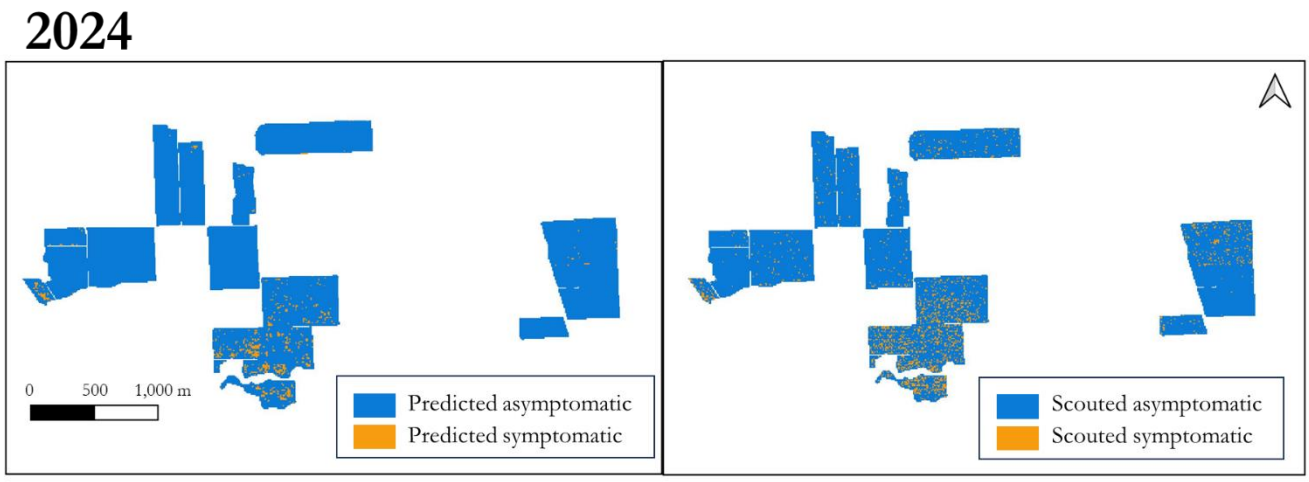

Figure 5: Random forest classifier predictions for GLRaV-3 symptomatic vine rate using Sentinel-2 MSI Imagery of August and September 2024 compared to scouting data in Lodi, CA area.

To determine the reliability of this model, we used several statistics, including class 1 recall, precision, and F1 score. Class 1 recall was 32.5%, meaning our model missed approximately two-thirds of symptomatic pixels. Precision was 38.6%, indicating that when the model predicted symptoms, it was correct less than 40% of the time. The F1 score was 0.35, reflecting the model's low reliability for GLRaV-3 symptom identification. These results were the product of several iterations, with various hyper parameters and feature combinations. These iterations showed little to no change in model performance.

3.2 Errors & Uncertainties

Training data limitations likely introduced error into the models. The scouting data were limited to a subset of vineyards, only covering roughly 1.3% of vineyard acreage in Lodi, and was based on visual identification of symptoms. While scouts were rigorously trained to identify GLRaV-3 symptoms, visual identification is not as reliable as lab testing due to disease latency and other confounding causes of leaf reddening. The rasterized scouting data also had a very skewed distribution, with many pixels containing low numbers of symptomatic vines and few pixels containing high numbers of symptomatic vines. While we attempted to account for this by grouping the scouting data into binary classes and heavily undersampling the majority class, we did not achieve completely balanced classes. Additionally, our conversion from the number of symptomatic vines in a pixel to the percentage of symptomatic vines in a pixel relied on vine spacing assumptions, which are not consistent across all vineyards.

Another potential source of error was the lack of differentiation between red grape varieties and white grape varieties in the statewide crop map. As a result, our model predicted across both red and white grape variety vineyards when it was trained on only scouting data from red grape variety vineyards. Additionally, due to the fact that satellite imagery is captured from a nadir view and grapevines are trellised, EMIT and Sentinel-2 imagery only capture the upper canopy of leaves. This likely introduced some uncertainty to our models, as symptoms do not always occur evenly across all canopy layers.

4. Conclusions

4.1 Interpretation of Results

Although the EMIT model's low class 1 precision (~24.7%) suggests that it overclassifies areas with greater than or equal to 1% symptomatic vines, anecdotal evidence from our partners at the LWC suggests that it may actually be underclassifying the true distribution of symptoms observed in Lodi. This indicates to us that while the EMIT model shows potential to be a tool to monitor GLRaV-3 associated symptoms, as evidenced by its strong class 1 recall (74.1%), the current model does not accurately predict on-the-ground conditions across the entire Lodi region. The EMIT model predictions for 2022–2024 show significant interannual variation (Figure 2). Specifically, a much greater area is classified as class 1 in 2022 than in 2023 and 2024. We hypothesize that this may be related to the drought that extended into 2022, which was followed by higher precipitation overall in 2023 (Wilmot, 2023). The model could be picking up on more drought-induced plant stress in 2022, causing it to overclassify areas as having ≥1% symptomatic vines. Limitations like these mean that the model is not ready for industry use; however, the model provides a foundation for future applications of EMIT in viticulture.

The Sentinel-2 random forest results indicate a substantial imbalance in detection capability between non-symptomatic and symptomatic pixels. Despite the model's high accuracy (~92.4%), its 32.5% recall means that the model misses approximately two-thirds of symptomatic pixels, which makes this approach insufficient as a standalone method for mapping disease spread. It is possible that early-stage GLRaV-3 symptoms may not produce strong enough spectral signatures that can be captured with Sentinel-2's multispectral bands to reliably separate symptomatic pixels from unknown ones. PSRI and NDRE were the most important features in the Sentinel-2 model (Figure B1-B2). Given that these two features were used as a proxy for plant stress, the model may be picking up on the spectral signatures of plants experiencing change due to confounding stressors such as drought. Relying on this methodology alone could give growers false confidence while undetected infections continue spreading through mealybug vectors, potentially worsening the virus. Overall, despite Sentinel-2's finer spatial resolution, the model performed worse than the EMIT model at identifying class 1 pixels. The disparity in model performance suggests that spectral resolution can be weighed higher than spatial resolution for GLRaV-3 symptom monitoring with EO technology.

While EMIT is a relatively new sensor designed for monitoring mineral dust, this study is among the first to demonstrate its potential utility for agricultural purposes. EMIT's coarse spatial resolution lacks the specificity to inform vine-scale management decisions, but its fine spectral resolution enables greater differentiation of subtle spectral changes associated with symptoms of viral infection. These findings suggest that with deeper

research and ground-truthing, EMIT may be useful in large-scale monitoring of agricultural disease challenges.

4.2 Feasibility & Partner Implementation

Hyperspectral imagery has previously been used in plant stress and disease detection, but scalable GLRaV-3 symptom detection has remained in question. Although there are limitations, we demonstrated that it is logical to continue to explore the use of EMIT hyperspectral imagery to inform agricultural management decisions. We found that while Sentinel-2 offers finer spatial resolution, its limited spectral resolution makes it unsuitable for GLRaV-3 symptom detection. In contrast, EMIT successfully captures spectral differences between high and low symptomatic areas that are invisible to the human eye, despite its coarser spatial resolution. Still, the EMIT detection model faces spatial constraints; each pixel contains approximately 2,400 grapevines, creating uncertainty about the precise location of symptomatic plants within each pixel. Importantly, while we used a threshold of 1% GLRaV-3 associated symptoms to separate symptomatic classes and train the EMIT model, a designation of greater than 1% symptoms may be less relevant for growers as management decisions are typically made for vineyards that display higher symptomatic rates. Though it is still far from individual infected vine identification, this technology could help reduce field visits and expensive vine testing by offering greater clarity on widespread GLRaV-3 conditions. EMIT, which can detect miniscule changes in vegetation spectra, represents a powerful tool that could one day benefit agricultural stakeholders facing similar challenges with disease monitoring.

5. Acknowledgements

Thank you to Katie Miller for your guidance throughout the DEVELOP program. Thank you to Dr. Stephanie Bolton for sharing your expertise on viticulture and Lodi. Thank you to Dr. Katie Gold, Dr. Shivranjani Baruah, Dr. Dana Chadwick, Dr. Allison Bredder, and Dr. Morgan Gilmour for your science advising support.

This material contains modified Copernicus Sentinel data (2022–2024), processed by ESA.

Any opinions, findings, and conclusions or recommendations expressed in this material are those of the authors and do not necessarily reflect the views of the National Aeronautics and Space Administration.

This material is based upon work supported by NASA through contract 80LARC23FA024.

6. Glossary

API – Application programming interface
AVA – American viticulture association
AVIRIS-NG – Airborne Visible/Infrared Imaging Spectrometer Next Generation
EMIT – Earth Surface Mineral Dust Source Investigation, hyperspectral sensor on the International Space Station
EO – Earth Observations, satellites and sensors that collect information about the Earth's physical, chemical, and biological systems over space and time
ESA – European Space Agency
EVI – Enhanced Vegetation Index, vegetation greenness index (modification of NDVI)
F1 score – model performance metric equal to the harmonic mean of precision and recall
GEE – Google Earth Engine, platform for accessing and analyzing EO
GLRaV-3 – Grapevine leafroll-associated virus complex 3
GLT – Geographic Lookup Table, data product used to translate crosstrack and downtrack coordinates into latitude and longitude
ISS – International Space Station
LWC – Lodi Winegrape Commission, a viticultural organization in California
MSI – Multispectral Instrument, multispectral sensor on Sentinel-2 satellite
Nadir – Direction pointing directly downward from a satellite
NASA Acres – consortium dedicated to supporting the U.S. agrifood system
NDRE – Normalized Difference Red Edge Index, vegetation health index
NDVI – Normalized Difference Vegetation Index, vegetation greenness index
NDWI – Normalized Difference Water Index, proxy for water content
PCA – Principal Component Analysis, technique used to reduce dimensionality
Precision – model performance metric indicating what percentage of the pixels predicted as a class actually belong to that class
PSRI – Plant Senescence Reflectance Index, vegetation health index
Recall – model performance metric indicating what percentage of the pixels that belong to a class are correctly predicted as that class

7. References

Alcohol and Tobacco Tax and Trade Bureau (2025). *Lodi AVA Shapefile* [Dataset]. U.S. Department of Treasury. https://www.ttb.gov/regulated-commodities/beverage-alcohol/wine/ava-map-explorer.

Australian Wine Research Institute. (2021, May). Grapevine leafroll-associated virus 3. *awri.com*. https://www.awri.com.au/wp-content/uploads/2021/05/Grapevine-leafroll-associated-virus-3-fact-sheet.pdf

Barnes, Edward., Clarke, T.R. & Richards, S.E. & Colaizzi, Paul & Haberland, Julio & Kostrzewski, M. & Waller, Peter & Choi, Christopher & Riley, E. & Thompson, T.L. (2000). Coincident detection of crop water stress, nitrogen status, and canopy density using ground based multispectral data. https://www.cabidigitallibrary.org/doi/full/10.5555/20023117563

Bolch, E. (2024). e*mit_tools:* Emit data processing library [Computer software]. NASA. https://github.com/nasa/EMIT-Data-Resources/blob/main/python/modules/emit_tools.py

Bolton, S. (2020). *What Every Winegrower Should Know: Viruses*. Lodi Winegrape Commission.

Bolton, S. (2023, June 5). *Why it's particularly difficult to protect your vineyard from mealybugs and viruses in California*. Lodi Wine Growers. https://lodigrowers.com/why-its-particularly-difficult-to-protect-your-vineyard-from-mealybugs-viruses-in-california/

Bolton, S. (2025, March 31). *Sniffing out threats: Dogs detect mealybugs & viruses in vineyards*. Lodi Wine Growers. https://lodigrowers.com/sniffing-out-threats-dogs-detect-mealybugs-viruses-in-vineyards/

California Department of Food and Agriculture. (2024). *State of California*. 2023–2024 California Agricultural Statistics Review. https://www.cdfa.ca.gov/Statistics/PDFs/2023-2024_california_agricultural_statistics_review.pdf

California Department of Water Resources. (2023). *Provisional 2023 Statewide Crop Mapping GIS Shapefile* [Dataset]. California Natural Resources Agency Open Data. https://data.cnra.ca.gov/dataset/statewide-crop-mapping

Caparoso, R. (2024). *Early report and favorite photographs of the start of the 2024 Lodi harvest*. Lodi Winegrape Commission. https://www.lodiwine.com/blog/Early-report-on-the-2024-Lodi-harvest

Gillies, S., & others. (2013-). Rasterio: geospatial raster I/O for Python programmers. Mapbox. https://github.com/rasterio/rasterio

h5netcdf Developers. (2024). *h5netcdf* (Version 1.7.3) [Computer software]. https://github.com/h5netcdf/h5netcdf

Huete, A., Didan, K., Miura, T., Rodriguez, E.P., Gao, X., & L.G. Ferreira. (2002). Overview of the radiometric and biophysical performance of the MODIS vegetation indices. *Remote Sensing of the Environment, 83*(1-2), 195-213. https://doi.org/10.1016/S0034-4257(02)00096-2

Kriegler, F., Malila, W., Nalepka, R., & Richardson, W. (1969). Preprocessing transformations and their effect on multispectral recognition. Proceedings of the 6th International Symposium on Remote Sensing of Environment. Ann Arbor, MI: University of Michigan, 97-131.

Lemaitre, G., Nogueira, F., & Aridas, C.K. (2017). Imbalanced-learn: A Python toolbox to tackle the curse of imbalanced datasets in machine learning. *Journal of Machine Learning Research, 18, 17,* 1-5. http://jmlr.org/papers/v18/16-365.html

Lodi Winegrape Commission. (2025). *Lodi Winegrape Commission – About.* https://www.lodiwine.com/About

Maree, H. J., Almeida, R. P. P., Bester, R., Chooi, K. M., Cohen, D., Dolja, V. V., Fuchs, M. F., Golino, D. A., Jooste, A. E. C., Martelli, G. P., Naidu, R. A., Rowhani, A., Saldarelli, P., & Burger, J. T. (2013). Grapevine leafroll-associated virus 3. *Frontiers in Microbiology*, *4*. https://doi.org/10.3389/fmicb.2013.00082

McFeeters, S.K. (1996). The use of the Normalized Difference Water Index (NDWI) in the delineation of open water features. *International Journal of Remote Sensing, 17*(7), 1425-1432. https://doi.org/10.1080/01431169608948714

Merzlyak, M.N., Gitelson, A.A., Chivkunova, O.B. & Rakitin, V.Y. (1999). Non-destructive optical detection of pigment changes during leaf senescence and fruit ripening. *Physiologia Plantarum, 106*, 135-141. https://doi.org/10.1034/j.1399-3054.1999.106119.x

Nguyen, C., Sagan, V., Maimaitiyiming, M., Maimaitijiang, M., Bhadra, S., & Kwasniewski, M. T. (2021). Early detection of plant viral disease using hyperspectral imaging and deep learning. *Sensors*, *21*(3), 742. https://doi.org/10.3390/s21030742

Pedregosa, F., Varoquaux, G., Gramfort, A., Michel, V., Thirion, B., Grisel, O., Blondel, M., Prettenhofer, P., Weiss, R., Dubourg, V., Vanderplas, J., Passos, A., Cournapeau, D., Brucher, M., Perrot, M., & Duchesnay, E. (2011). Scikit-learn: Machine learning in Python. *Journal of Machine Learning Research*, *12*, 2825–2830.

Portela, F., Sousa, J. J., Araújo-Paredes, C., Peres, E., Morais, R., & Pádua, L. (2024). A systematic review on the advancements in remote sensing and proximity tools for grapevine disease detection. *Sensors*, *24*(24), 8172. https://doi.org/10.3390/s24248172

Romero Galvan, F. E., Pavlick, R., Trolley, G., Aggarwal, S., Sousa, D., Starr, C., Forrestel, E., Bolton, S., Alsina, M. del M., Dokoozlian, N., & Gold, K. M. (2023). Scalable early detection of grapevine viral infection with airborne imaging spectroscopy. *Phytopathology*, *113*(8), 1439–1446. https://doi.org/10.1094/PHYTO-01-23-0030-R

Sawyer, E., Laroche-Pinel, E., Flasco, M., Cooper, M. L., Corrales, B., Fuchs, M., & Brillante, L. (2023). Phenotyping grapevine red blotch virus and grapevine leafroll-associated viruses before and after symptom expression through machine-learning analysis of hyperspectral images. *Frontiers in Plant Science*, *14*, 1117869. https://doi.org/10.3389/fpls.2023.1117869

Wilmot, B. (2023, March 13). *Lodi Wine Country Winter 2022-23 Recap & Spring 2023 Outlook. Lodi Wine Growers.* https://lodigrowers.com/lodi-wine-country-winter-2022-23-recap-spring-2023-outlook/

Yildirim, F., & Kaya, A. (2008). Selecting map projections in minimizing area distortions in GIS applications. *Sensors, 8*(12), 7809-7817. https://doi.org/10.3390/s8127809

8. Appendices

Appendix A: *Model Accuracy Maps*

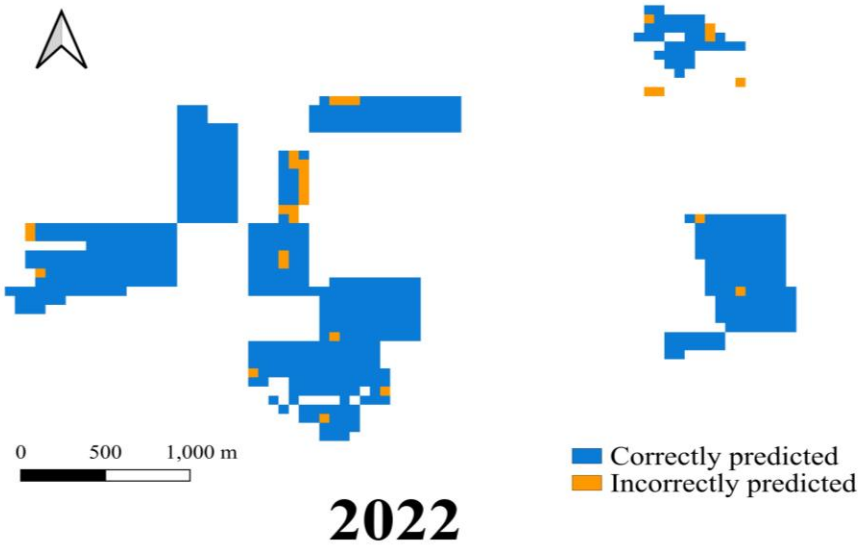

Figure A1. 2022 model accuracy map for a subset of Lodi comparing scouting data with model predictions. Correctly predicted pixels are shown in blue and incorrectly predicted pixels are shown in orange.

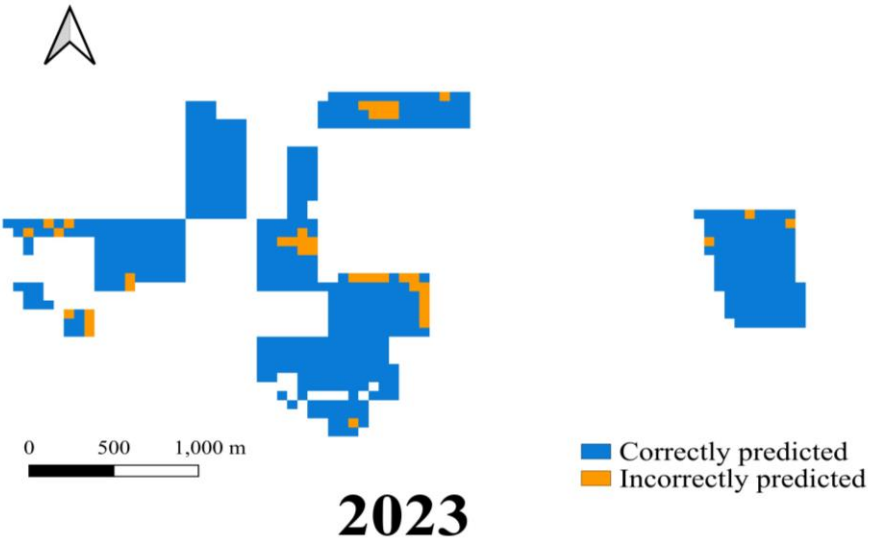

.

Figure A2. 2023 model accuracy map for a subset of Lodi comparing scouting data with model predictions. Correctly predicted pixels are shown in blue and incorrectly predicted pixels are shown in orange.

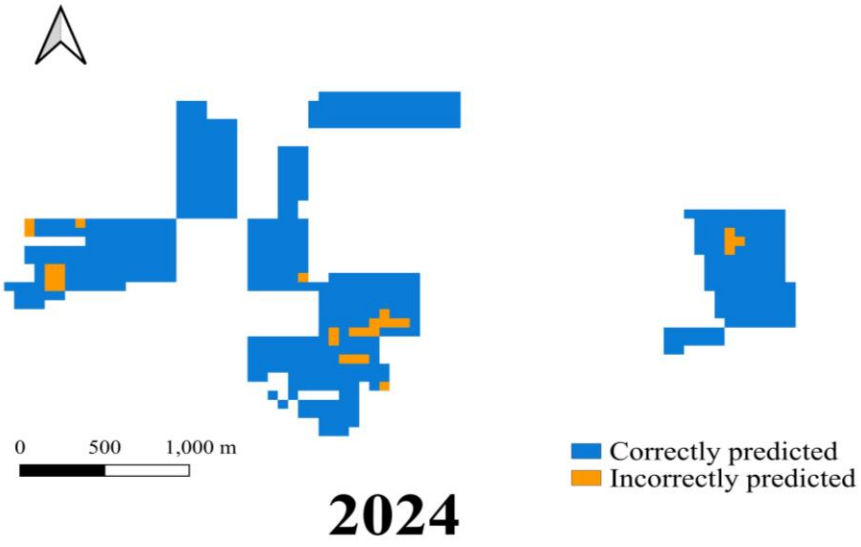

Figure A3. 2024 model accuracy map for a subset of Lodi comparing scouting data with model predictions. Correctly predicted pixels are shown in blue and incorrectly predicted pixels are shown in orange.

Appendix B: *Sentinel-2 Index Maps*

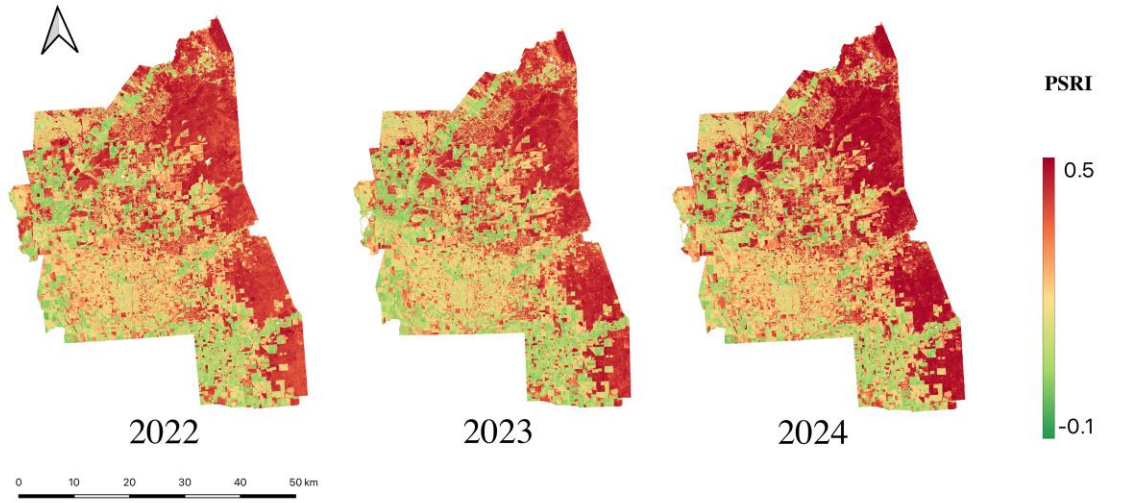

Figure B1. PSRI for Sentinel-2 is calculated using a composite image for August-September each year from 2022–2024. Lower values are shown in green and high values in red.

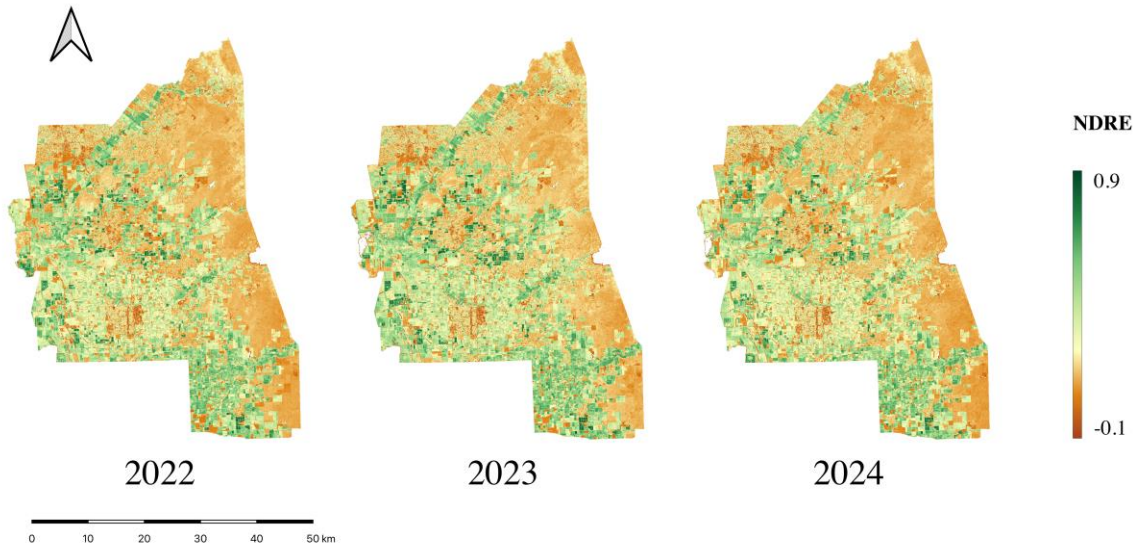

Figure B2. NDRE for Sentinel-2 is calculated using a composite image for August-September each year from 2022–2024. Lower values are shown in red and high values in green.